Forecasting deflation, intrusion and eruption at inflating volcanoes

Journal Item

Elsevier Editorial System(tm) for Earth and Planetary Science Letters

Manuscript Draft

Manuscript Number: EPSL-D-17-00572R2

Title: Forecasting deflation, intrusion and eruption at inflating volcanoes

Article Type: Letters

Keywords: eruption forecasting; conditional probability; Krafla

Corresponding Author: Dr. Steve Blake, BSc, PhD

Corresponding Author's Institution: The Open University

First Author: Steve Blake, BSc, PhD

Order of Authors: Steve Blake, BSc, PhD; Joaquin Cortes

Abstract: A principal goal of volcanology is to successfully forecast the start of volcanic eruptions. This paper introduces a general forecasting method, which relies on a stream of monitoring data and a statistical description of a given threshold criterion for an eruption to start. Specifically we investigate the timing of intrusive and eruptive events at inflating volcanoes. The gradual inflation of the ground surface is a well-known phenomenon at many volcanoes and is attributable to pressurized magma accumulating within a shallow chamber. Inflation usually culminates in a rapid deflation event caused by magma escaping from the chamber to produce a shallow intrusion and, in some cases, a volcanic eruption. We show that the ground elevation during 15 inflation periods at Krafla volcano, Iceland, increased with time towards a limiting value by following a decaying exponential with characteristic timescale τ. The available data for Krafla, Kilauea and Mauna Loa volcanoes show that the duration of inflation (t^*) is approximately equal to τ. The distribution of t^*/τ values follows a log-logistic distribution in which the central 60% of the data lie between $0.99 < t^*/\tau < 1.76$. Therefore, if τ can be constrained during an on-going inflation period, then the cumulative distribution function of t^*/τ values calibrated from other inflation periods allows the probability of a deflation event starting during a specified time interval to be estimated. The time window in which there is a specified probability of deflation starting can also be forecast, and forecasts can be updated after each new deformation measurement. The method provides stronger forecasts than one based on the distribution of repose times alone and is transferable to other types of monitoring data and/or other patterns of pre-eruptive unrest.

Forecasting deflation, intrusion and eruption at inflating volcanoes

Stephen Blake[1] and Joaquin A. Cortés[2,3]

[1]School of Environment, Earth and Ecosystem Sciences, The Open University, Walton Hall, Milton Keynes MK7 6AA, UK (corresponding author; Stephen.Blake@open.ac.uk)

[2]Department of Geography, Edge Hill University, Ormskirk, L39 4QP, UK

[3]School of Geosciences; The University of Edinburgh; Grant Institute. The King's Buildings, James Hutton Road, Edinburgh EH9 3JW, UK.

Abstract

A principal goal of volcanology is to successfully forecast the start of volcanic eruptions. This paper introduces a general forecasting method, which relies on a stream of monitoring data and a statistical description of a given threshold criterion for an eruption to start. Specifically we investigate the timing of intrusive and eruptive events at inflating volcanoes. The gradual inflation of the ground surface is a well-known phenomenon at many volcanoes and is attributable to pressurized magma accumulating within a shallow chamber. Inflation usually culminates in a rapid deflation event caused by magma escaping from the chamber to produce a shallow intrusion and, in some cases, a volcanic eruption. We show that the ground elevation during 15 inflation periods at Krafla volcano, Iceland, increased with time towards a limiting value by following a decaying exponential with characteristic timescale τ. The available data for Krafla, Kilauea and Mauna Loa volcanoes show that the duration of inflation (t^*) is approximately equal to τ. The distribution of t^*/τ values follows a log-logistic distribution in which the central 60% of the data lie between $0.99 < t^*/\tau < 1.76$. Therefore, if τ can be constrained during an on-going inflation period, then the cumulative distribution function of t^*/τ values calibrated from other inflation periods allows the probability of a deflation event starting

during a specified time interval to be estimated. The time window in which there is a specified probability of deflation starting can also be forecast, and forecasts can be updated after each new deformation measurement. The method provides stronger forecasts than one based on the distribution of repose times alone and is transferable to other types of monitoring data and/or other patterns of pre-eruptive unrest.

Keywords: Krafla, eruption forecasting, conditional probability

1. Introduction

Forecasting the onset, size, location, style and duration of a volcanic eruption is an important and challenging goal of volcanology. In terms of forecasting the start of an eruption, one approach is to use a time series of monitoring data to extrapolate to the time at which the measured parameter will reach a known threshold value at which an eruption starts (Chadwick et al., 2012; Nooner and Chadwick, 2016). The theoretical basis of this approach is exemplified by the materials failure forecast method (Voight, 1988) and relies on the eruption threshold condition being known precisely. This approach can, in principle, predict the time at which failure is reached, and an eruption starts. In practice, however, uncertainty in the data, in the model of the time-dependence of the measured quantity, in the fitting of data to a model, and in the extrapolation of the fitted trend result in uncertainty in the predicted eruption onset time, although the uncertainty diminishes with increasing time (Bell et al., 2011, 2013).

Alternatively, monitoring data can be used to make a judgement of the likelihood of an eruption starting within some future time window, such as "the next *N* days", rather than pin-pointing the eruption time. This type of approach may use a statistical analysis of a volcano's long-term record of repose periods (reviewed by Marzocchi and Bebbington, 2012), or interpretation of on-going short-term unrest (e.g., Swanson et al., 1983, 1985; Linde et al., 1993; Harlow et al., 1996; Chadwick et al., 2012; and reviews by Sparks, 2003; Bell et al., 2015; Pallister and McNutt, 2015). Useful measures of unrest for this purpose include the rates of seismicity (Voight, 1988; Cornelius and Voight, 1994,

1995; Kilburn 2012; Robertson and Kilburn 2016), changes in the seismic properties of the volcano (Brenguier et al., 2008; Chouet and Matoza, 2013; Crampin et al., 2015), the gas composition or emission rate (Carapezza and Federico, 2000; Laiolo et al., 2012; Aiuppa et al., 2007; Carapezza et al., 2009; de Moor et al., 2015), thermal remote sensing data (van Manen et al., 2013; Reath et al., 2016), crustal deformation (Linde et al., 1993) and ground surface deformation (Chadwick et al., 2012; Segall, 2013). Methods which combine two or more types of data have also been advocated (e.g., Klein, 1984; Schmid et al., 2012; Pallister and McNutt, 2015). Given an empirically-defined statistical model connecting the magnitude of unrest and the time remaining to an eruption onset, then quantitative probabilistic forecasts of an eruption starting within a particular time window can be made. An example is the forecasting of explosive eruptions during dome-forming episodes of Bezymianny volcano using thermal remote sensing data (van Manen et al., 2013). The forecasting of eruption duration using historical data (Sparks and Aspinall, 2004; Gunn et al., 2014; Wolpert et al., 2016) relies on the same type of analysis. This paper applies this statistics-based approach to the surface inflation that precedes eruptions and shallow intrusions, presenting general expressions for forecasting the probability of an event happening within any user-defined time interval.

In some cases, pre-eruptive surface inflation proceeds at a constant rate (e.g., Chaussard et al., 2013; Delgado et al., 2014; Champenois et al., 2014), whereas in other cases an exponentially decreasing rate of inflation has been measured such that tilt, vertical and horizontal displacement, or volume of the inflation dome follows

$$\Delta D = a\,(1 - \exp(-t/\tau)), \qquad (1)$$

where ΔD is the change in the measured deformational quantity since the start of inflation at time $t = 0$, a is a constant equal to the value of ΔD that would be attained at time $t = \infty$, and τ is a characteristic e-folding timescale (Dvorak and Okamura, 1987; Lu et al., 2003; Lengliné et al., 2008; Dzurisin et al., 2009). This behaviour is readily explained by physics-based models of the growing over-pressure within a replenished shallow magma chamber that is contained in elastic country rock and fed at a rate determined by the pressure gradient along the feeding conduit (Lengliné et al., 2008; Pinel et al.,

2010). Inflation, being proportional to chamber over-pressure, increases up to the point when a threshold over-pressure breaks open the chamber (Blake, 1981). Magma then escapes from the chamber, causing the ground surface to deflate, and a dyke propagates away from the chamber and may intercept the ground surface. The start of deflation is thus the time at which magma withdrawal starts and an intrusion is initiated, in some cases feeding an eruption. Whether an intrusion actually breaks the surface (and how long after the start of deflation, and where the location of any eruptive vents is) is likely to depend on magma properties, rock properties, crustal stress and topography, as explored in theoretical models by Buck et al., (2006), Heimisson et al., (2015a) and Pinel et al., (2017).

According to Eq. (1), if deflation is triggered when the amount of deformation is ΔD^*, then this happens at time t^* which is proportional to the exponential timescale (τ)

$$t^* = -\tau \ln(1 - \Delta D^*/a), \qquad (2)$$

This implies that if early monitoring data can constrain the value of τ, then a forecast of the time at which magma withdrawal starts, t^*, can be made within the limits of variation in $-\ln(1 - \Delta D^*/a)$.

In Section 2, Eq. (1) is fitted to inflation periods at Krafla volcano which preceded intrusions (as detected by seismic and deformational evidence) and, in some cases, eruptions. The results, together with published results from Kilauea and Mauna Loa, show that t^* seems to be proportional to τ, with the ratio t^*/τ falling in a narrow range. In Sections 3 and 4 the statistical distribution of t^*/τ values is used to calculate the probability that deflation will start within any user-defined time interval. We also calculate the size of the time window in which the probability has a particular value, and show how forecasts can be continuously updated on the basis of new monitoring data. Section 5 discusses how our method can be adapted to make the same type of forecasts using other types of pre-eruptive measurements that follow a given time-dependent function.

2. Ground inflation, deflation and eruptions at Krafla

The Krafla volcanic system is situated in Iceland's Northern Volcanic Zone. It has a 12-km diameter caldera and a system of ground fissures and vents which extend beyond the caldera to the North and South. An active geothermal system lies within the caldera. In 1975-1984 a repeated sequence of activity occurred in which gradual ground inflation centred within the caldera was interrupted by rapid deflation accompanied by rifting and sometimes basaltic eruptions (e.g., Björnsson et al., 1979; Ewart et al., 1990, 1991; Buck et al., 2006; Wright et al., 2012). Seismicity accompanying rifting has been interpreted to have resulted from dominantly lateral propagation of dykes carrying basaltic magma from a shallow magma chamber below the caldera. An S-wave shadow zone (Einarsson, 1978; Brandsdóttir and Menke 1992; Brandsdóttir et al., 1997) and modelling of ground deformation (e.g., Björnsson et al., 1979; Johnsen et al., 1980; Ewart et al., 1990, 1991; Heimisson et al., 2015b) place the shallow chamber, or a complex of magma storage compartments, at about 2 to 4 km depth.

Here, we investigate the record of ground inflation using the data on surface elevation provided by Björnsson and Eysteinnson (1998) (see Fig. 1) pertaining to levelling station FM5596 located about 1 km from the centre of deformation. Measurements were typically recorded on a daily to hourly basis. We designate as inflation period 1 the measured inflation which started in February 1976, following the end of the first eruptive event in the 1975-1984 activity, because this marks the start of frequent measurements of inflation. The elevation at which deflation started generally increased over time, rather than occurring at a more or less constant threshold elevation, as appears to be the case at Axial Seamount (Chadwick et al., 2012; Nooner and Chadwick, 2016). At Krafla, the threshold elevation is variable and is likely to be a function of time-dependent magmatic, tectonic and topographic stresses (Buck et al., 2006).

Of the 17 inflation periods which preceded deflation (Fig. 1), all but the two most recent periods (lasting from 04/02/1981 to 18/11/1981 and from 22/11/1981 to 04/09/1984) are described well by the single exponential function of Eq. (1). These are the 15 periods plotted in Fig. 2 and listed in Table 1. They lasted from tens of days to hundreds of days and inflation stopped (when deflation and eruption/intrusion started) after inflation of 0.2 to 1.2 m. Note that although elevation increases during each inflation period at a decreasing rate through time, some irregularity occurs because of occasional

rapid but small deflations and inflations. These are treated as noise because they are much smaller than the 0.1 to 1.05 m deflation events that accompany intrusions and eruptions. Fitting was done using the Levenberg-Marquardt algorithm (see Appendix A) and the best-fit parameter values are listed in Table 1; the time constant τ ranges from 13.7 to 537 days. Figure 3 shows a representative example of a fitted curve.

Inflations 16 and 17 followed a double exponential model which, as will be mentioned in the Discussion, we attribute to a viscoelastic response of the system after sufficiently long time (cf. Nooner and Chadwick, 2009). However, for the purposes of this paper, attention is focused on inflations described by Eq. (1).

3. Forecasting method

As already noted, Dvorak and Okamura (1987) and Lengliné et al. (2008) used Eq. (1) to describe some inflation episodes at Kilauea and Mauna Loa volcanoes. Combining their best-fit values of τ with the new results from Krafla (Table 1), Figure 4a compares the duration of inflation, t^*, with the exponential timescale, τ, for these three basaltic volcanoes. A strong correlation exists such that for given τ, the time when deflation starts, t^*, is likely to lie within a well-prescribed range. The correlation holds irrespective of whether the deflation was accompanied by an eruption or only an intrusion, as is expected if deflation is triggered at a critical threshold whereas an eruption requires an additional criterion related to dyke propagation dynamics, magma buoyancy and surface topography. The correlation between t^* and τ in Fig. 4a also appears to be independent of which volcano is involved, albeit with the caveat that more data from Kilauea, Mauna Loa and other volcanoes would be interesting.

That the Hawaiian and Krafla data have similar t^*/τ ratios is not unexpected for the following reason: In physical terms, for a magma chamber inflating due to the inflow of buoyant magma from below (e.g., Pinel et al., 2010), the critical amount of inflation ΔD^* is proportional to the critical over-pressure in the chamber (ΔP^*). The maximum permissible amount of inflation, a, is that which would be caused by an excess chamber pressure that balances the buoyancy of the magma in the feeder

conduit given by $g\Delta\rho L$ where g is the acceleration due to gravity, $\Delta\rho$ is the density difference between the magma and country rock, and L is the length of the feeder conduit. In such a model, t^*/τ = -ln(1-$\Delta P^*/g\Delta\rho L$) and a deflation will be triggered as long as $\Delta P^*/g\Delta\rho L < 1$. Choosing reasonable values for these parameters ($3 < \Delta P^* < 30$ MPa, $100 < \Delta\rho < 400$ kg m^{-3} and $5 < L < 20$ km) yields a spread of t^*/τ ratios that are confined within the range of about 0.07 to 5, which is consistent with Fig. 4. Although the ranges of physical parameter values, and hence t^*/τ ratios, within a given volcanic system are likely to be narrower, disparate volcanoes can still be expected to have t^*/τ values that overlap, as appears to be the case from Fig. 4. Thus, until more deformation data are available, the dispersion in the data represented by the pooled cumulative distribution function (cdf) in Fig. 4b is taken to describe the relationship between the duration (t^*) and time-constant (τ) of inflation at most volcanoes which behave according to Eq. (1).

The cumulative distribution function (cdf) of the ratio t^*/τ (Fig. 4b) is sigmoidal, such that deflation is more likely to start when t^*/τ is near the median value. A smoothed version of the empirical cdf can be calculated using a best-fit to a theoretical distribution, such as a log-logistic distribution. We consider this distribution because it is adequate for events whose rate increases initially and decreases later as exponential decay. The distribution has a sigmoidal shape and a simple 2-parameter definition:

$$cdf_{log-logistic} = \frac{1}{1+\left(\frac{(t^*/\tau)}{\alpha}\right)^{-\beta}} \quad , \qquad (3)$$

where α is the median value of t^*/τ and β is a shape factor. Values of $\alpha = 1.319$ and $\beta = 4.756$ were found by maximum likelihood estimation to approximate the empirical cdf, with the goodness of fit being validated using the Kolmogorov-Smirnov test. The empirical cdf of t^*/τ as well as the log-logistic fit are shown in Fig. 4b.

The cdf of t^*/τ can be used to calculate the probability of a deflation starting within a given time interval by applying the theory of conditional probability and using an estimate of τ found by fitting

Eq. (1) to on-going inflation data. Thus, at some time, t, after the start of an inflation period the probability of deflation starting between t_1 ($\geq t$) and t_2 ($> t_1$) is (see Appendix B)

$$p = \frac{CDF(t_2/\tau) - CDF(t_1/\tau)}{1 - CDF(t/\tau)} \ . \qquad (4)$$

We focus on the probability, evaluated at the elapsed time t, of deflation starting in the time window between t and $t + \Delta t$. In other words, at any current time during the course of on-going inflation, we wish to find the probability that a deflation event will start before a time period of length Δt has passed. Following Eq. (4), this is:

$$p = \frac{CDF\big((t+\Delta t)/\tau\big) - CDF(t/\tau)}{1 - CDF(t/\tau)} \ . \qquad (5)$$

Graphs showing how this probability changes over time, and for different values of Δt, are given in Fig. 5, where t and Δt are normalised by τ and the cdf is given by the log-logistic model in Eq. (3) and Fig. 4b. Figure 5a makes the obvious point that the probability increases with an increasing size of time window, $\Delta t/\tau$. For given $\Delta t/\tau$, the probability of deflation happening within that time window is initially low; this is because the cdf is relatively flat at small times, and increases as the steepest portion of the cdf is approached, which is when t/τ is close to the median value of t^*/τ. At later times, if deflation has not yet happened, the probability decreases once the long tail of the cdf is reached because a given size of time window contains a diminishingly small proportion of the cdf.

Fig. 5(b) shows that the shortest time interval associated with a given probability is reached when t/τ is close to the median value of t^*/τ. This is where the cdf is steepest, such that a given proportion of t^*/τ values is contained within the shortest time span. The shortest time interval with a probability greater than 0.5 is initially $\Delta t/\tau = 1.32$ (because this is the median value of t^*/τ) and falls to $\Delta t/\tau = 0.3$ at $t/\tau = 1.5$.

4. A retrospective illustration of probabilistic forecasting in real time

As shown above, the probabilities of deflation starting in a given time window can be calculated from the cdf as a function of the dimensionless time t/τ. To express the size of these time windows in

absolute terms requires knowledge of τ, and this is estimated by fitting Eq. (1) to deformation data obtained up to time t ($< t^*$). This is designated as $\tau(t)$ to distinguish it from the values of τ (Table 1, Fig. 4) which are calculated based on all measurements in an inflation period. The fitting method is described in Appendix A.

Using inflation period 9 (τ = 121 days, t^* = 177 days) for illustration, irregularities in the elevation data cause the best fit values of $\tau(t)$ to vary during the course of inflation (Fig. 6) but inevitably the locus of (t, $\tau(t)$) points moves towards the region of Fig. 4(a) occupied by (t^*, τ) values, and t^*/τ ratios, which characterise the start of deflations. The time evolution of forecasts will therefore reflect any change in $\tau(t)$ as well as the passage of time on the conditional probabilities.

In applying the forecasting method, a user may be interested in the probability of a deflation starting in a given time interval or, conversely, the time interval which carries a given probability. In the former case, continually updated conditional probabilities are calculated using Eq. (5) with τ replaced by $\tau(t)$ as shown in Fig. 7a for inflation 9. In the alternative case, Equations (3) and (5) are rearranged to find Δt for given p:

$$\Delta t = \tau(t)\alpha\left(\frac{p+\left(\frac{1}{\alpha}\frac{\Delta t}{\tau(t)}\right)^{\beta}}{1-p}\right)^{1/\beta} - t \ , \qquad (6)$$

The results from this calculation are shown in Fig. 7b.

Both plots in Fig. 7 show variation due to variation in $\tau(t)$ superimposed on the trends found in the normalised plots for constant τ in Fig. 5. For example, the major changes at early times in Fig. 7a,b are mainly due to changes in the best fit value of $\tau(t)$ shown in Fig. 6. Once $\tau(t)$ becomes more stable, the trends in Fig. 7 more closely follow the theoretical curves of Fig. 5 in which the probability of a deflation in a given size of time window increases until $t \approx \tau$, and then gradually decreases. Likewise, the length of the time window associated with a given probability decreases until $t \approx \tau$ and then slowly increases.

It may seem counter-intuitive that the probability does not continue to increase while more and more time goes by without a deflation event. However, there are two reasons why the probability of deflation starting within a time window of given length (as opposed to deflation starting at any time which, in our model is $p = 1$) eventually decreases if a deflation event has not happened after a sufficiently long time.

The first is that the probabilities are calculated from a model distribution that by definition extends to infinite time. In other words, there is no known or assumed upper limit to how long inflation will continue. If there was a finite time by which deflation must start, then the probability would indeed increase as that time was approached, but here there is no such constraint.

The probabilities depend on the shape of the cdf. In particular, the log-logistic distribution has a long tail in which the slope of the cdf decreases as the cdf asymptotes to 1 as time tends to infinity. This contrasts with the shape of the cdf at early times, which shows the slope of the cdf increasing. This shape reflects the fact that the distribution of t^*/τ values has a central peak straddled by shallow tails, as illustrated by the clustering of data points in Figure 4a.

Secondly, then, the proportion of the population of all deflation start times contained within a time window that lies in the long tail of the distribution is small and becomes smaller as t tends to infinity and the cdf asymptotes to 1. This is the opposite of the trend at earlier times, when the proportion increases according to the steepening of the cdf.

The probability (Eq. 5) depends on the ratio of the proportion of the population of all deflation start times that lies between t and Δt, divided by the proportion of the population that lies beyond the present time. These proportions are $(\mathrm{cdf}(t/\tau + \Delta t/\tau) - \mathrm{cdf}(t/\tau))$ and $(1 - \mathrm{cdf}(t/\tau))$ respectively. The former term increases as the cdf curve steepens (up to the median time) and decreases as the cdf curve flattens out (after the median time). The latter term always decreases with time. Consequently, at early times the probability increases and at later times decreases.

Figure 7 also illustrates how the method can be used. After 30 days of inflation, there is a 40% chance of deflation starting in the next 50 days (i.e., before the 80th day after this inflation period started) and only a 2% chance that it starts in the next 10 days. As time passes without deflation and with the gathering of more deformation data that allows $\tau(t)$ to be re-calculated with more data, the probabilities associated with given time windows are continually updated. After 130 days, there is a 68% chance of deflation happening in the next 50 days, and a 20% chance of deflation in the next 10 days.

Alternatively, specifying an 80% probability of deflation starting, the model forecasts a time window that decreases from about 100 days to 70 days as inflation continues to the 130th day. Thereafter, the length of the time window increases once $t >> \tau$ as a consequence of the cdf of t^*/τ flattening, as explained in Section 3. A trade-off between high probabilities being associated with long time windows and a desire to anticipate a deflation event within a short time window but with high probability is met when the times and time windows are of order $\tau \times$ the median value of the t^*/τ ratio, in this case 1.32 τ. In other words, the strongest forecasts are made around the times when the curves in Figs. 5a and 7a reach high values and when the curves in Figs. 5b and 7b reach low values.

5. Discussion

This section compares the model with other approaches and explains how it can be used with data which follow a different time-dependence from the decaying exponential of Eq. (1). First, we remark on a caveat that applies to all eruption forecasting methods which is that geophysical unrest need not lead inevitably to an eruption (Moran et al., 2011), because the priming mechanism may cease before a given critical threshold is reached. A survey by Biggs et al. (2014) found that of the 54 volcanoes which showed surface deformation detected by InSAR in the previous 18 years, 25 erupted whereas 29 did not erupt. Of their 34 studied volcanoes which did erupt, 9 did so without accompanying deformation. The reasons for these varied behaviours probably relate to tectonic setting and the depth of magma bodies (Biggs et al., 2014) and the detectability of the surface expression of sub-surface

275 volume or mass changes within complex magma plumbing systems of varying size and location
276 (Biggs and Pritchard, 2017; Sparks and Cashman, 2017).

277 The forecasting approach introduced here can be compared with one based only on the distribution of
278 inflation durations (t^*). Fig. 8 compares the empirical cdfs of t^* and of t^*/τ for the 15 inflation periods
279 of Krafla. It shows that the t^*/τ cdf has a narrower central portion, indicating that including the extra
280 information provided by a value of τ allows better discrimination of when deflation is likely to start.
281 Indeed, the cdf of t^* values is close to a straight line, such that t^* values between the minimum and
282 maximum values are equally likely whereas the sigmoidal log-logistic cdf of t^*/τ implies that t^*/τ will
283 be more likely to lie in a narrower range. A further advantage of the new model is that the distribution
284 of normalised inflation times, t^*/τ, appears to be general whereas the distribution of t^* values is
285 volcano-specific.

286 We reiterate that our method forecasts the onset of deflation whether or not the subsequent intrusion
287 produced an eruption. At Krafla, the 15 inflation periods which followed Eq. (1) all culminated in an
288 intrusion but only 6 of them produced an eruption. While separate cdfs for inflation episodes which
289 preceded eruptive and non-eruptive deflations could be made in order to allow separate forecasts of
290 the probabilities of the timing of eruptive and non-eruptive deflations (on the assumption that
291 eruptions happen randomly in any sequence of deflation events), the small amount of available data
292 precludes this. However, the empirical evidence of Fig. 4a is that eruptive and non-eruptive deflations
293 are not associated with different populations of t^*/τ values. This is consistent with the expectation that
294 the condition for an eruption to happen at some time during deflation is independent of the condition
295 for deflation to start.

296 The t^*/τ method introduced here applies only to inflations which follow Eq. (1), in other words,
297 volcanoes with inflation at an exponentially decreasing rate. The procedure of updating fits to Eq. (1)
298 as more monitoring data are collected allows the user to continually judge whether Eq. (1) adequately
299 fits the data. If it does, then the forecasting method using Eqs. (4) and (5) and the cdf shown in Fig. 4b
300 remain valid. However, if Eq. (1) becomes inadequate, then the forecasting method should be

modified. Inflation histories that are described by equations other than Eq. (1) (Nooner and Chadwick, 2009; Reverso et al., 2014; Le Mével et al., 2015, 2016; Carrier et al., 2015) may reflect additional processes or boundary conditions but can in principle be treated using Eqs. (4) and (5) if an appropriate scaling of the eruption time (t^*) can be found and the cdf of the scaled eruption time can be defined.

For example, inflation episodes 16 (from 04/02/1981 to 18/11/1981, t^* = 286 days) and 17 (from 22/11/1981 to 04/09/1984, t^* = 1018 days) at Krafla show systematic departures from the single exponential model of Eq. (1). Figure 9a,b shows that they are more clearly described by the double exponential model

$$\Delta D = a_1(1 - \exp(-t/\tau_1)) + a_2(1 - \exp(-t/\tau_2)), \quad (7)$$

which Nooner and Chadwick (2009) used to describe inflation of Axial Seamount between its eruptions in 1998 and 2011. The second exponential term only becomes necessary after long times and may arise when the system starts to respond in a viscoelastic way. As with the single exponential model, given sufficient data, it would be possible to define a cdf of t^*/τ_2 (where $\tau_2 > \tau_1$) and then use it in the forecast model of Eq. 4.

In general, the approach based on Eq. (4) can be applied in any situation where a physical measure, Q, of pre-eruptive unrest (e.g., ground elevation, tilt, earthquake rate) is monitored and obeys a time-dependent function $f(t/T)$, where T is a constant normalising time-scale whose value can be estimated by fitting $Q = f(t/T)$ to monitoring data. The function f can be empirical or be based on a physics-based model, such as pressurisation of an elastic magma chamber (as in Eq. (1)) and inelastic deformation (wherein the inverse of the rate of elevation change decreases linearly with time ($f \propto (1 - t/T)$; Robertson and Kilburn (2016)). Given a number of past eruptions happening at known t^* and T, then the cdf of t^*/T can be plotted and described by the best fit to an appropriate reference distribution (e.g., log-logistic, Weibull, normal etc). The best-fit cdf then defines the population of t^*/T values at which eruptions begin. The probability of an eruption starting within any user-defined time window, given that some amount of time t has already passed, can then be calculated by applying Eq. (4), the

value of T having been found through fitting $Q = f(t/T)$. The value of T and the probability can be continually updated in real-time as monitoring data accrues.

6. Conclusions

Motivated by the need for improved quantitative probabilistic forecasting methods for volcanic eruptions, we introduce a method which produces forecasts of the type "The probability that a deflation will start during the next N days is p". The method requires monitoring data and a statistical description of the threshold conditions for an eruption (or other event) to start. In our case, the time at which an inflating volcano starts to deflate, a process which initiates a shallow intrusion that sometimes leads to an eruption, is parameterised by an exponential timescale (τ) describing the time-dependence of inflation rate. In particular, we have shown that Eq. (1) describes inflation episodes at Krafla volcano which are followed by deflation, intrusion and in some cases, eruption. Certain inflation episodes at Kilauea and Mauna Loa also follow Eq. (1) (Dvorak and Okamura, 1987; Lengliné et al., 2008). The pooled data show that the duration of inflation t^* is proportional to the exponential timescale τ, and the ratio t^*/τ follows a log-logistic distribution with median of ca. 1.3 and 20% and 80% percentile values of ca. 0.99 and ca. 1.78. The cdf of t^*/τ allows the probability that deflation will start within a given user-defined time window to be calculated (Eqs. (4) and (5) and Figs. 5 and 7). Probabilities can be continually updated in real-time as more deformation data become available during an ongoing inflation period because this allows the value of τ to be continually refined. The method performs better than forecasts based solely on the statistics of t^* values. The methodology is transferable to any time-dependent pre-eruptive monitoring data for which the cdf of the duration of unrest (t^*) scaled by a time-scale, T, is known and for which a value of T can be determined from on-going monitoring data.

Acknowledgements

We thank Leanne Gunn and Chris McDonald for transcribing data from Björnsson and Eysteinnson (1998), and Eliza Calder and Saskia van Manen for helpful comments on an earlier draft. We

appreciate the constructive reviews by William Chadwick and an anonymous reviewer, as well the Editor, Tamsin Mather, whose comments helped to clarify the paper. This research did not receive any specific grant from funding agencies in the public, commercial, or not-for-profit sectors.

References

Aiuppa, A., Moretti, R., Federico, C., Guidice, G., Gurrieri, S., Papale, P., Shinohara, H., Valenza, M., 2007. Forecasting Etna eruptions by real-time observation of volcanic gas composition. Geology 35, 1115-1118, doi: 10.1130/G24149A.1

Bell, A.F., Naylor, M., Heap, M.J., Main, I.G., 2011. Forecasting volcanic eruptions and other material failure phenomena: An evaluation of the failure forecast method. Geophysical Research Letters 38(15), L15304.

Bell, A.F., Naylor, M., Main, I.G., 2013. The limits of predictability of volcanic eruptions from accelerating rates of earthquakes. Geophysical Journal International 194, 1541-1553.

Bell, A.F., Kilburn, C.R.J., Main, I.G., 2015. Volcanic eruptions, Real-time forecasting of. *In* M. Beer, I.A., Kougioumtzoglou, E., Patelli and S.-K. Au, (eds.) Encyclopedia of Earthquake Engineering, 3892-3906, Springer-Verlag, Berlin, doi:10.1077/978-3-642-36197-5_43.

Biggs, J., Ebmeier, S.K., Aspinall, W.P., Lu, Z., Pritchard, M.E., Sparks, R.S.J., Mather, T.A., 2014. Global link between deformation and volcanic eruption quantified by satellite imagery. Nature Communications, doi:10.1038/ncomms4471.

Biggs, J., Pritchard, M.E., 2017. Global volcano monitoring: what does it mean when volcanoes deform? Elements 13,17-22, doi:10.2113/gselements.13.1.17

Björnsson, A., Eysteinsson, H., 1998. Breytingar á landhæð við Kröflu 1974-1995. Samantekt á landhæðarmælingum. Orkustofnun report OS-98002.

Björnsson, A., Johnsen, G., Sigurdsson, S., Thorbergsson, G., 1979. Rifting of the plate boundary in North Iceland 1975-1978. Journal of Geophysical Research 84, 3029-3038.

377 Blake, S., 1981. Volcanism and the dynamics of open magma chambers. Nature 289, 783-785.

378 Brandsdóttir, B., Menke, W.H., 1992. Thin low-velocity zone within the Krafla caldera, NE-Iceland
379 attributed to a small magma chamber. Geophysical Research Letters 19, 2381-2384.

380 Brandsdóttir, B., Menke, W., Einarsson, P., White, R.S., Staples, R.K., 1997. Faroe-Iceland Ridge
381 Experiment 2. Crustal structure of the Krafla central volcano. Journal of Geophysical Research 102,
382 7867-7886.

383 Brenguier, F., Shapiro, N.M., Campillo, M., Ferrazzini, V., Duputel, Z., Coutant, O., Nercessian, A.,
384 2008. Towards forecasting volcanic eruptions using seismic noise. Nature Geoscience 1, 126-130.

385 Buck, W.R., Einarsson, P., Brandsdóttir, B., 2006. Tectonic stress and magma chamber size as
386 controls on dike propagation: Constraints from the 1975-1984 Krafla rifting episode. Journal of
387 Geophysical Research 111, B12404, doi: 10.1029/2005JB003879.

388 Carapezza, M.L., Federico, C., 2000. The contribution of fluid geochemistry to the volcano
389 monitoring of Stromboli. Journal of Volcanology and Geothermal Research 95, 227–245.

390 Carapezza, M.L., Ricci, T., Ranaldi, M., Tarchini, L., 2009. Active degassing structures of Stromboli
391 and variations in diffuse CO_2 output related to the volcanic activity. Journal of Volcanology and
392 Geothermal Research 182, 231–245.

393 Carrier, A., Got, J.L., Peltier, A., Ferrazzini, V., Staudacher, T., Kowalski, P., Boissier, P., 2015. A
394 damage model for volcanic edifices: Implications for edifice strength, magma pressure, and eruptive
395 processes. Journal of Geophysical Research Solid Earth 120, 567-583, doi:10.1002/2014JB011485.

396 Chadwick, W.W., Nooner, S.L., Butterfield, D.A., Lilley, M.D., 2012. Seafloor deformation and
397 forecasts of the April 2011 eruption at Axial Seamount. Nature Geoscience 5, 474-477, doi:
398 10.1038/NGEO1464

399 Champenois, J., Pinel, V., Baize, S., Audin, L., Jomard, H., Hooper, A., Alvarado, A., Yepes, H.,
400 2014. Large-scale inflation of Tungurahua volcano (Ecuador) revealed by Persistent Scatterers SAR
401 interferometry. Geophysical Research Letters 41, 5821-5828, doi: 10.1002/2014GL060956.

Chaussard, E., Amelung, F., Aoki, Y., 2013. Characterization of open and closed volcanic systems in Indonesia and Mexico using InSAR time series. Journal of Geophysical Research: Solid Earth 118, 3957-3969, doi: 10.1002/jgrb.50288.

Chouet, B., Matoza, R.S., 2013. A multi-decadal view of seismic methods for detecting precursors of magma movement and eruption. Journal of Volcanology and Geothermal Research 252(15), 108-175.

Cornelius, R.R., Voight, B., 1994. Seismological aspects of the 1989–1990 eruption at Redoubt Volcano, Alaska: the Materials Failure Forecast Method (FFM) with RSAM and SSAM seismic data. Journal of Volcanology and Geothermal Research 62(1-4), 469-498

Cornelius, R.R., Voight, B., 1995. Graphical and PC-software analysis of volcano eruption precursors according to the Materials Failure Forecast Method (FFM). Journal of Volcanology and Geothermal Research 64(3-4), 295-320.

Crampin, S., Gao, Y., Buckits, J., 2015. A review of retrospective stress-forecasts of earthquakes and eruptions. Physics of the Earth and Planetary Interiors 245, 76-87, doi: 10.1016/j.pepi.2015.05.008.

Delgado, F., Pritchard, M.E., Lohman, R., Naranjo, J.A., 2014. The 2011 Hudson volcano eruption (Southern Andes, Chile): Pre-eruptive inflation and hotspots observed with InSAR and thermal imagery. Bulletin of Volcanology 76, 815, doi: 10.1007/s00445-014-0815-9

De Moor, J.M., Aiuppa, A., Avard, G., Wehrmann, H., Dunbar, N., Muller, C., Tamburello, G., Giudice, G., Liuzzo, M., Moretti, R., Conde, V., Galle, B., 2016. Turmoil at Turrialba Volcano (Costa Rica): Degassing and eruptive processes inferred from high-frequency gas monitoring. Journal of Geophysical Research Solid Earth 121, 5761-5775, doi:10.1002/2016JB013150.

Dvorak, J.J., Okamura, A.T., 1987. A hydraulic model to explain variations in summit tilt rate at Kilauea and Mauna Loa Volcanoes. In Volcanism in Hawaii (RW Decker, TL Wright and PH Stauffer eds) vol 2 USGS Prof Paper 1350, Chapter 46, 1281-1296.

425 Dzurisin, D., Lisowski, M., Wicks, C.W., 2009. Continuing inflation at Three Sisters volcanic center,
426 central Oregon Cascade Range, USA, from GPS, levelling, and InSAR observations. Bulletin of
427 Volcanology 71, 1091-1110, doi:10.1007/s00445-009-0296-4.

428 Einarsson, P., 1978. S-wave shadows in the Krafla caldera in NE-Iceland, evidence for a magma
429 chamber in the crust. Bulletin Volcanologique 41, 1-9.

430 Ewart, J.A., Voight, B., Björnsson, A., 1990. Dynamics of Krafla caldera, north Iceland: 1975-1985.
431 *In* Magma Transport and Storage, (M.P. Ryan, *ed*) 225-276. John Wiley and Sons Ltd.

432 Ewart, J.A.,Voight, B., Björnsson, A., 1991. Elastic deformation models of Krafla Volcano, Iceland,
433 for the decade 1975 through 1985. Bulletin of Volcanology 53, 436-459.

434 Gunn, L.S., Blake, S., Jones, M.C., Rymer, H., 2014. Forecasting the duration of volcanic eruptions:
435 an empirical probabilistic model. Bulletin of Volcanology 76, 780, DOI 10.1007/s00445-013-0780-8

436 Harlow, D.H., Power, J.A., Laguerta, E.P., Ambubuyog, G., White, R.A., Hoblitt, R.P., 1996.
437 Precursory seismicity and forecasting of the June 15, 1991, eruption of Mount Pinatubo. Fire and
438 Mud: eruptions and lahars of Mount Pinatubo, Philippines, pp. 223-247.

439 Heimisson, E.R., Hooper, A., Sigmundsson, F., 2015a. Forecasting the path of a laterally propagating
440 dike. Journal of Geophysical Research. Solid Earth 120, 8774-8792. doi: 10.1002/2015JB012402.

441 Heimisson, E.R., Einarsson, P., Sigmundsson, F., Brandsdóttir, B., 2015b. Kilometer-scale Kaiser
442 effect identified in Krafla volcano, Iceland. Geophysical Research Letters 42, 7958-7965, doi:
443 10.1002/2015GL065680

444 Johnsen, G.V., Björnsson, A., Sigurdsson, S., 1980. Gravity and elevation changes caused by magma
445 movement beneath the Krafla caldera, Northeast Iceland. Journal of Geophysics 47, 132-140.

446 Kilburn, C., 2012. Precursory deformation and fracture before brittle rock failure and potential
447 application to volcanic unrest. Journal of Geophysical Research 117, B02211,
448 doi:10.1029/2011JB008703.

449 Klein, F., 1984. Eruption forecasting at Kilauea Volcano, Hawaii. Journal of Geophysical Research:
450 Solid Earth 89(B5), 3059-3073, doi: 10.1029/JB089iB05p03059.

451 Laiolo, M., Cigolini, C., Coppola, D., Piscopo, D., 2012. Developments in real-time radon monitoring
452 at Stromboli volcano. Journal of Environmental Radioactivity 105, 21–29.

453 Le Mével, H., Feigl, K.L., Córdova, L., DeMets, C., Lundgren, P., 2015. Evolution of unrest at
454 Laguna del Maule volcanic field (Chile) from InSAR and GPS measurements, 2003-2014.
455 Geophysical Research Letters 42, 6590-6598, doi: 10.1002/2015GL064665.

456 Le Mével, H., Gregg, P.M., Feigl, K.L., 2016. Magma injection into a long-live reservoir to explain to
457 explain geodetically measured uplift: Application to the 2007-2014 unrest episode at Laguna del
458 Maule volcanic field (Chile). Journal of Geophysical Research 121, 6092-6108, doi:
459 10.1002/2016JB013066

460 Lengliné, O., Marsan, D., Got, J.L., Pinel, V., Ferrazzini, V., Okubo, P.G., 2008. Seismicity and
461 deformation induced by magma accumulation at three basaltic volcanoes. Journal of Geophysical
462 Research 113, B12305, doi:10.1029/2008JB005937.

463 Levenberg, K., 1944. A Method for the Solution of Certain Non-Linear Problems in Least Squares.
464 Quarterly of Applied Mathematics 2, 164–168.

465 Linde, A.T., Agustsson, K., Sacks, I.S., Stefansson, R., 1993. Mechanism of the 1991 eruption of
466 Hekla from continuous borehole strain monitoring. Nature 365, 737-740, doi: 10.1038/365737a0

467 Lu, Z., Masterlark, T., Dzurisin, D., Rykhus, R., Wicks Jr., C., 2003. Magma supply dynamics at
468 Westdahl volcano, Alaska, modelled from satellite radar interferometry. Journal of Geophysical
469 Research 108, doi:10.1029/2002JB002311.

470 Marquardt, D., 1963. An Algorithm for Least-Squares Estimation of Nonlinear Parameters. SIAM
471 Journal on Applied Mathematics 11, 431–441.

472 Marzocchi, W., Bebbington, 2012. Probabilistic eruption forecasting at short and long time scales.
473 Bulletin of Volcanology 74, 1777-1805.

474 Moran, S.C., Newhall, C., Roman, D.C. 2011. Failed magmatic eruptions: late-stage cessation of
475 magma ascent. Bulletin of Volcanology 73, 115-122.

476 Nooner, S.L., Chadwick Jr., W.W., 2009. Volcanic inflation measured in the caldera of Axial
477 Seamount: implications for magma supply and future eruptions. Geochemistry, Geophysics,
478 Geosystems 10(2) Q02002, doi:10.1029/2008GC002315.

479 Nooner, S.L., Chadwick Jr., W.W., 2016. Inflation-predictable behaviour and co-eruption deformation
480 at Axial Seamount. Science 354, 1399-1403. doi: 10.1126/science.aah4666

481 Pallister, J., McNutt, S.R., 2015. Synthesis of Volcano Monitoring. *In* Encyclopedia of Volcanoes,
482 (Sigurdsson, H., Houghton, B., McNutt, S., Rymer, H. and Stix, J. *Eds.*). pp 1151-1171.

483 Pinel, V., Jaupart, C. J., Albino, F., 2010. On the relationship between cycles of eruptive activity and
484 growth of a volcanic edifice. Journal of Volcanology and Geothermal Research 194, 150-164.

485 Pinel, V., Carrara, A., Maccaferri, F., Rivalta, E., Corbi, F., 2017. A two-step model for dynamical
486 dike propagation in two dimensions: Application to the July 2001 Etna eruption. Journal of
487 Geophysical Research. Solid Earth 122, 1107–1125, doi:10.1002/2016JB013630

488 Reath, K.A., Ramsey, M.S., Dehn, J., Webley, P.W., 2016. Predicting eruptions from precursory
489 activity using remote sensing data hybridization, Journal of Volcanology and Geothermal Research
490 321, 18-30, doi: 10.1016/j.jvolgeores.2016.04.027.

491 Reverso, T., Vandemoulebrouck, J., Jouanne, F., Pinel, V., Villerin, T., Sturkell, E., Bescou, P., 2014.
492 A two-magma chamber model as a source of deformation at Grimsvötn volcano, Iceland. Journal of
493 Geophysical Research 119, 4066-4083. doi: 10.1002/2013JB010569

494 Robertson, R.M. Kilburn, C.R.J., 2016. Deformation regime and long-term precursors to eruption of
495 large calderas: Rabaul, Papua New Guinea. Earth and Planetary Science Letters 438, 86-94.

496 Schmid, A., Grasso, J.R., Clarke, D., Ferrazzini, V., Bachèlery, P., Staudacher, T., 2012. Eruption
497 forerunners from multiparameter monitoring and application for eruptions time predictability (Piton
498 de la Fournaise). Journal of Geophysical Research 117, B11203, doi:10.1029/2012JB009167.

499 Segall, P., 2013. Volcano deformation and eruption forecasting. *In* Remote sensing of volcanoes and
500 volcanic processes: integrating observation and modelling, (Pyle, D.M, Mather, T.A., Biggs, J., *Eds.*).
501 Geological Society Special Publications, 380, 85-106. doi:10.1144/SP380.4.

502 Sparks, R.S.J., 2003. Forecasting volcanic eruptions. Earth and Planetary Science Letters 210, 1-15.

503 Sparks, R.S.J., Aspinall, W.P., 2004. Volcanic activity: Frontiers and challenges in forecasting,
504 prediction and risk assessment. In The State of the Planet: Frontiers and Challenges in Geophysics.
505 Geophysical Monograph 150, 359-373. IUGG and American Geophysical Union,
506 doi:10.1029/150GM28

507 Sparks, R.S.J., Cashman, K.V., 2017. Dynamic Magma Systems: Implications for Forecasting
508 Volcanic Activity. Elements, 13, 35-40.

509 Swanson, D.A., Casadevall, T.J., Dzurisin, D., Malone, S.D., Weaver, C.S., 1983. Predicting
510 eruptions at Mount St. Helens, June 1980 through December 1982. Science 221, 1369-1376.

511 Swanson, D.A., Casadevall, T.J., Dzurisin, D., Holcomb, R.T., Newhall, C.G., Malone, S.D., Weaver,
512 C.S., 1985. Forecasts and predictions of eruptive activity at Mount St Helens, USA: 1975-1984.
513 Journal of Geodynamics 3, 397-423.

514 van Manen, S., Blake, S., Dehn, J., Valcic, L., 2013. Forecasting large explosions at Bezymianny
515 volcano using thermal satellite data. *In* Remote sensing of volcanoes and volcanic processes:
516 integrating observation and modelling, (Pyle, D.M, Mather, T.A., Biggs, J., *Eds*), Geological Society
517 Special Publications, 380, 187-201, doi:10.1144/SP380.3.

518 Voight, B., 1988. A method for prediction of volcanic eruptions. Nature 332, 125-130.

519 Wolpert, R.L., Ogburn, S.E., Calder, E.S., 2016. The longevity of lava dome eruptions. Journal of
520 Geophysical Research 121, 676-686, doi: 10.1002/015JB012435

521 Wright, T.J., Sigmundsson, F., Pagli, C., Belachew, M., Hamling, I.J., Brandsdottir, B., Keir, D.,
522 Pedersen, R., Ayele, A., Ebinger, C., Einarsson, P., Lewi, E., Calais, E., 2012. Geophysical
523 constraints on the dynamics of spreading centres from rifting episodes on land. Nature Geoscience 5,
524 242-250, doi: 10.1038/ngeo1428

525

Table 1: Inflation periods considered in this study from Krafla, Mauna Loa and Kilauea volcanoes. Kilauea 1977-1979 and Mauna Loa parameters are from Lengliné et al. (2008). Puu O'o' values are from Dvorak and Okamura (1987). *a values are given in [m] units except Puu O'o' given in [μ rad] units ("N/A" when the values were not reported).

Inflation	Start date (dd-mm-yy)	Duration (t*) [days]	τ [days]	a []*	t*/τ
Krafla 1	15-02-76	227.63	537.12	3.954	0.42
Krafla 2	04-10-76	26.83	23.34	0.234	1.15
Krafla 3	01-11-76	79.16	99.67	1.089	0.79
Krafla 4	21-01-77	95.89	77.79	0.827	1.23
Krafla 5	28-04-77	132.82	111.5	1.174	1.19
Krafla 6	14-09-77	114.79	79.23	0.893	1.45
Krafla 7	25-01-78	166.10	160	1.603	1.04
Krafla 8	12-07-78	120.79	139.2	1.193	0.87
Krafla 9	15-11-78	178.88	121.3	1.090	1.47
Krafla 10	18-05-79	258.58	85.06	0.840	3.04
Krafla 11	19-02-80	26.05	13.71	0.070	1.90
Krafla 12	17-03-80	115.33	51.25	0.635	2.25
Krafla 13	16-07-80	94.86	61.49	0.528	1.54
Krafla 14	23-10-80	60.98	41.9	2.561	1.46
Krafla 15	29-12-80	32.29	21.53	0.222	1.50
Mauna Loa 1975-1984 (Lengliné et al, 2008)	06-07-75	3184.31	2670	N/A	1.19
Kilauea 1977-1979 (Lengliné et al, 2008)	01-10-77	605.05	412.45	N/A	1.47
Kilauea between Puu O'o' Episodes 3 and 4	09-04-83	65.31	40	32*	1.63

(Dvorak and Okamura, 1987)					

526

527 **Figure Captions**

528 **Figure 1**: Elevation above sea level of station FM5596 at Krafla (data from Björnsson and
529 Eysteinnson (1998)) showing the 17 periods (represented with different colours for clarity) of gradual
530 inflation followed by rapid deflation. Deflation events that were accompanied by an eruption are
531 indicated with a red star.

532 **Figure 2.** Change in elevation during inflation periods 1 to 15 at Krafla (see Table 1), plotted from
533 data in Björnsson and Eysteinsson (1998). Time and elevation change are referenced to the first data
534 point in each inflation period, which was within a few hours or at most days of the start of inflation, as
535 identified by other means. Colours as in Figure 1.

536 **Figure 3.** Plot of elevation change since the start of Krafla inflation period 9 and, in red, the best fit to
537 equation (1) found using the Levenberg-Marquardt algorithm.

538 **Figure 4.** (a) Log-log plot of t^* versus τ, the $t^*/\tau = 0.9852$ and $t^*/\tau = 1.7648$ blue lines define the
539 envelope around the central 60% of the data as shown in panel (b). Filled symbols refer to inflation
540 events that culminated in a shallow intrusion which fed an eruption, open symbols refer to inflation
541 events that culminated in a non-eruptive intrusion. (b) Cumulative distribution function of t^*/τ with
542 best-fit log-logistic distribution in red (Eq. (3)) and parameter values $\alpha = 1.318539$ and $\beta = 4.756239$.
543 Blue lines with $t^*/\tau = 0.9852$, 1.31068 and 1.7648 represent 20%, 50% and 80% probability
544 respectively.

545 **Figure 5.** Relationships between the probability at elapsed time t, of deflation starting within the next
546 Δt, evaluated using equation (5) and the log-logistic model. (a) The probability, as a function of time
547 t/τ, of deflation starting within the next $\Delta t/\tau$. (b) The time interval $\Delta t/\tau$ within which there is a given
548 probability of deflation starting, plotted as a function of time t/τ.

549 **Figure 6.** Plot, akin to Fig. 4a but using linear axes and using data for Krafla inflation period 9,
550 showing how $\tau(t)$ can vary over time and that $t/\tau(t)$ increases to values encountered at the start of

551 deflation. 60% of deflation start when ($\tau(t^*)$, t^*) plots between the lines $t/\tau(t)$ = 0.9852 and 1.764 (i.e.
552 cdf = 0.2 and 0.8, as in Fig. 4b).

553 **Figure 7.** Forecasts for Krafla inflation period 9 in terms of the relationships between the probability,
554 at elapsed time *t*, of deflation starting within the next Δt, evaluated using Eq. (5) and the log-logistic
555 model. (a) The probability of deflation starting in the next period Δt, as a function of time *t*. Different
556 colours indicate deflation starting within the next 10 (black), 20 (red), 30 (blue), 50 (green) or 100
557 (magenta) days. (b) The time interval Δt, as a function of time, associated with a 20% (green), 40%
558 (blue), 60% (red) and 80% (black) probability of deflation starting, calculated using Eq. (6).

559 **Figure 8**. Comparison of the cdfs of t^* (blue) and t^*/τ (red) for inflation periods 1 to 15 of Krafla,
560 plotted by normalising to the maximum value in each case.

561 **Figure 9** Inflation 16 and 17 of Krafla volcano, showing single exponential fits (Eq. (1), red lines)
562 and double exponential fit (Eq. 9, blue lines). (a) Inflation 16, with best fit parameters a = 0.452 m
563 and τ = 71.32 days with a single exponential fit and a_1 = 0.2347 m, τ_1 = 23.5323 days, a_2 = 1.7458 m,
564 τ_2 = 1822.9611 days with a double exponential fit. **(b)** Inflation 17, with best fit parameters a = 0.699
565 m and τ = 114.426 days for a single exponential fit, and a_1 = 0.3661 m, τ_1 = 20.7144 days, a_2 =
566 0.5561m, τ_2 = 613.736 days with a double exponential fit.

567

568 **Appendix A Parameter estimation**

569 Estimation of the parameters a and τ is performed using the Levenberg-Marquardt (Levenberg, 1944;
570 Marquardt, 1963) non-linear least-squared regression on the inflation data at a given time and
571 inflation t_i *and* Δh_i. The algorithm is an iterative method based on finding the vector of parameters β =
572 (a, τ) that minimize the sum of the squares of deviation $S(\beta)$ from the model curve $f(t, \beta)$:

573 $$S(\beta) = \sum_{i=1}^{m} [\Delta h_i - f(t_i - \beta)]^2 \qquad \text{(A.1)}$$

Starting with an initial guess of $\beta = (a_0, \tau_0)$, the values are updated on iteration steps by replacing β by a new estimate $\beta + \delta$ in which δ is calculated from the set of linear equations resulting from the minimization of a relaxed version of the Jacobian of $f(t, \beta)$. In general, if n parameters are unknown, the method requires at least $n + 1$ data points to converge, e.g. in theory at least three data points are required to solve for the two parameters a and τ. In practical terms, the iterative process requires many more data points to find a meaningful solution, i.e. with values of a and τ lying within realistic windows, as the algorithm finds local minima values and those can be spurious. We therefore apply cut-off criteria based on the following arguments:

First, as we want to examine an exponential model rather than a linear one, $t/\tau(t)$ shouldn't be too small (i.e. not << 1). Second, as very large values of $t/\tau(t)$ in Eq. (1) imply that inflation will cease after a very short time we regard any $\tau(t)$ values such that $t/\tau(t) > 10$ as unrealistic. We therefore only accept $\tau(t)$ values if $0.1 \leq t/\tau(t) \leq 10$.

Appendix B Conditional Probability

Calculating the probability of deflation starting (at time t^*) within some specified time interval, given that an amount of time $t < t^*$ has passed is a particular case of calculating the conditional probability of the occurrence of an event A given that an event B has already happened: P(A|B). It is well known that:

$$P(A|B) = \frac{P(A \cap B)}{P(B)} \qquad \text{(B.1)}$$

i.e. this conditional probability is equal to the probability of the combined event divided by the probability of the event that has happened. In our case, defining the probability of deflation at a given time t^* after a given amount of time t has occurred implies that $A = t \leq t^* \leq t + \Delta t$ and $B = t^* > t$. Because $A \cap B = t < t^* \leq t + \Delta t$ (i.e. the probability of the combined event is equal to the probability of the eruption happening after t) and $P(t^* > t)$ is the definition of the survivor function, Eq. B.1 can be rewritten as:

598 $$P(t \leq t^* \leq t + \Delta t | t^* > t) = \frac{P(t < t^* < t+\Delta t)}{1-P(t)} \qquad \text{(B.2)}$$

599 To calculate these probabilities, we first estimate the cumulative distribution function of t^*/τ, based on

600 the values of t^*/τ of previous inflations to assess the conditional probability as:

601 $$P(t \leq t^* \leq t + \Delta t | t^* > t) = \frac{CDF\left(\frac{t+\Delta t}{\tau}\right) - CDF\left(\frac{t}{\tau}\right)}{1-CDF\left(\frac{t}{\tau}\right)} \qquad \text{(B.3)}$$

602

Figure

Click here to download high resolution image

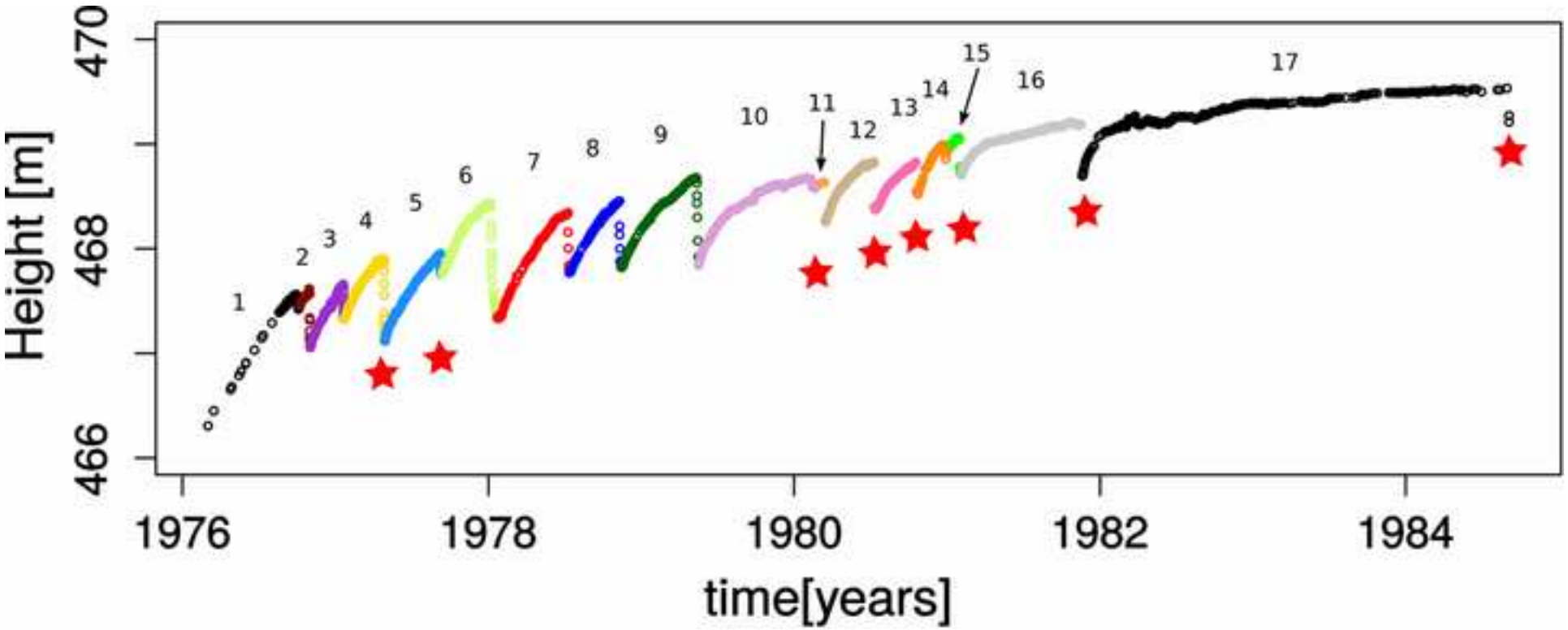

Figure

Click here to download high resolution image

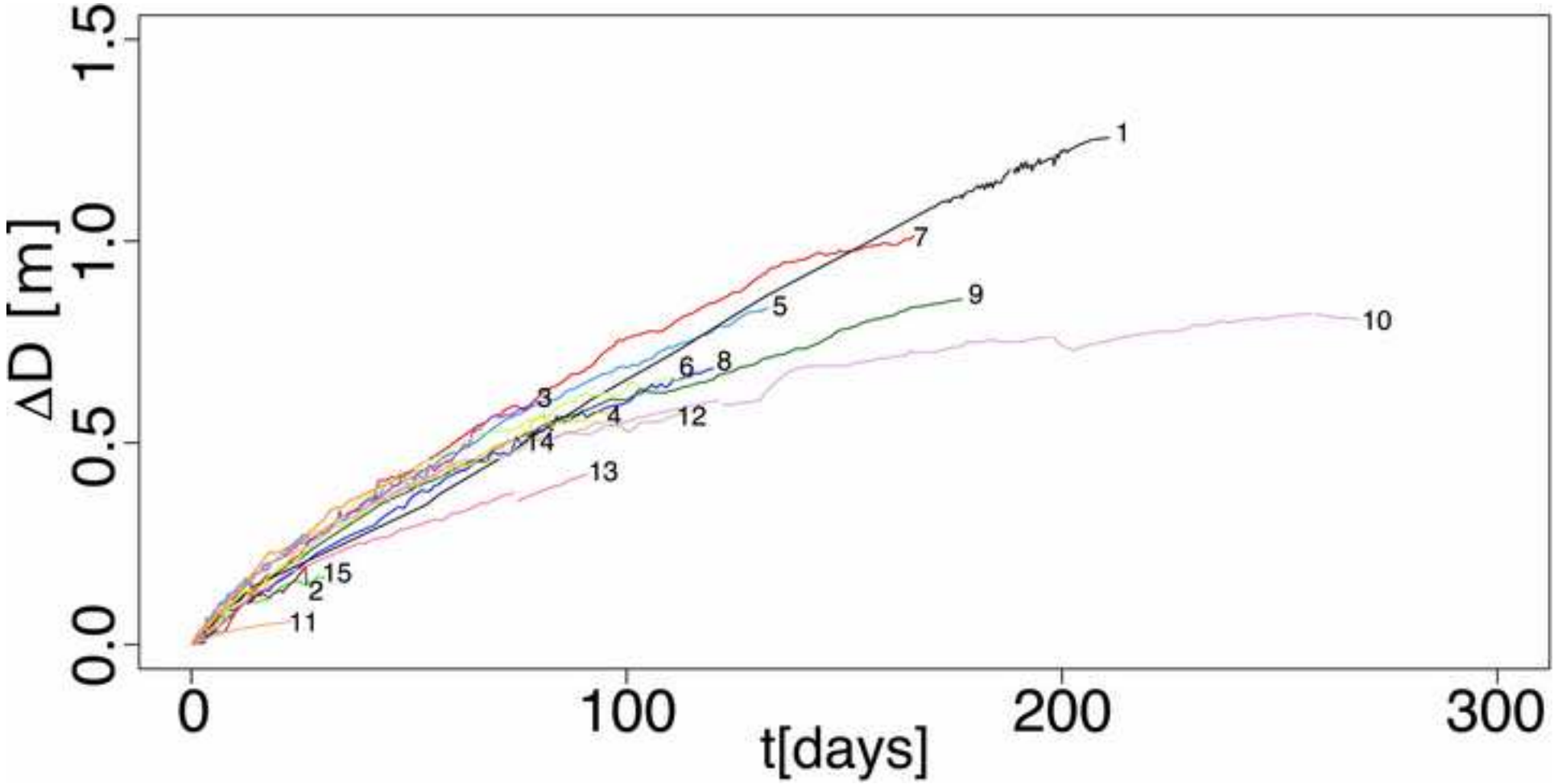

Figure
Click here to download high resolution image

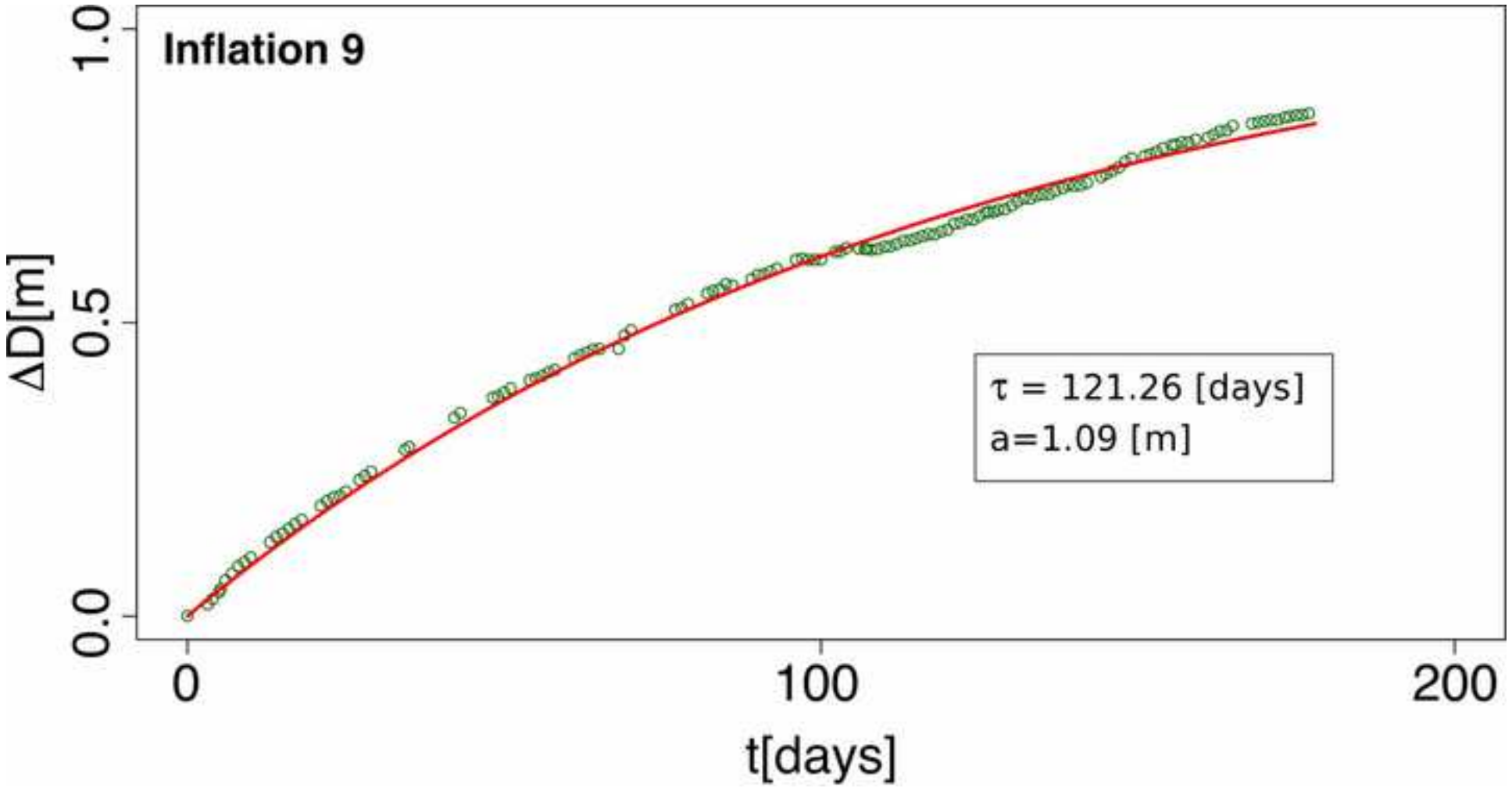

Figure

Click here to download high resolution image

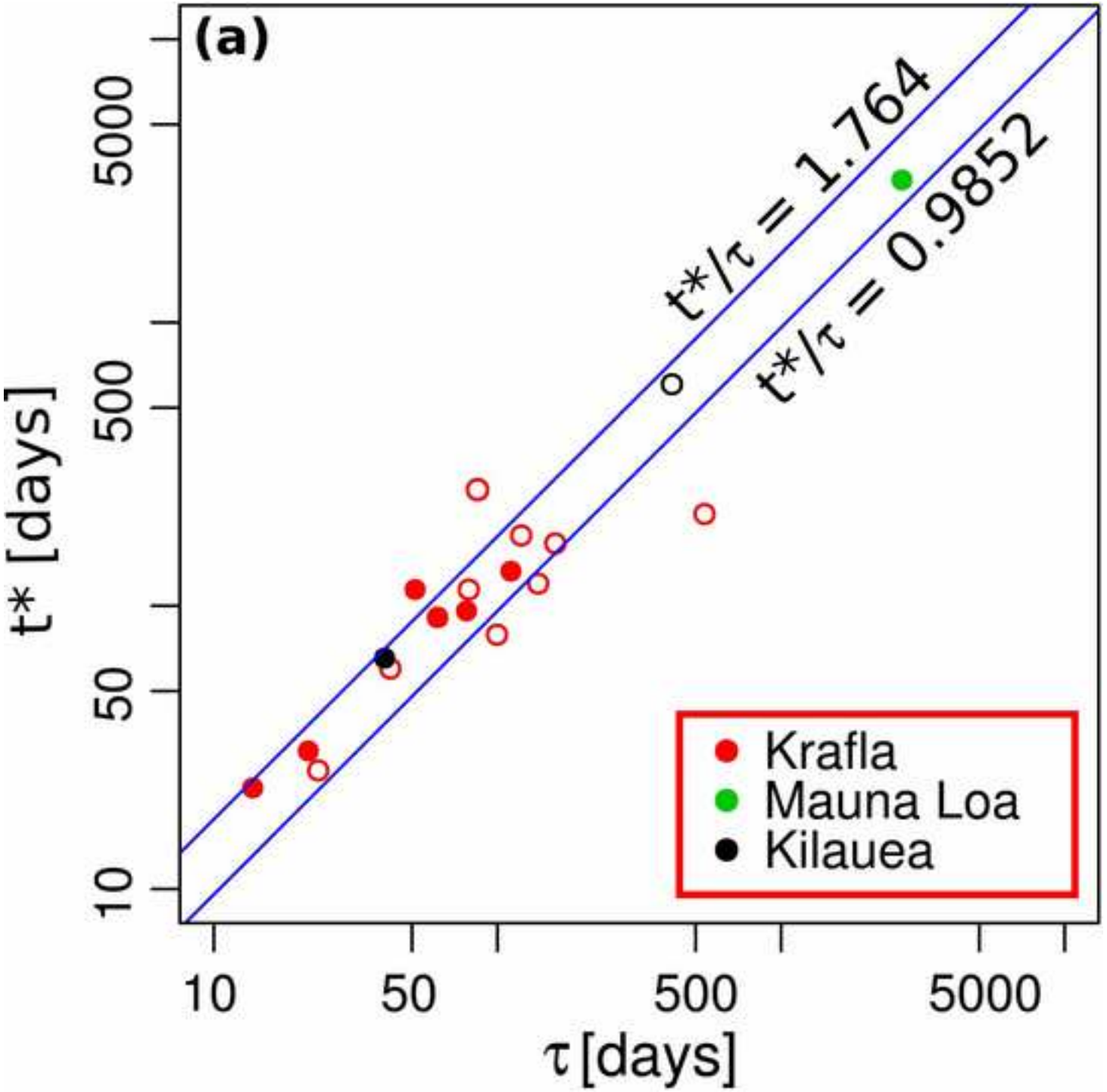

Figure

Click here to download high resolution image

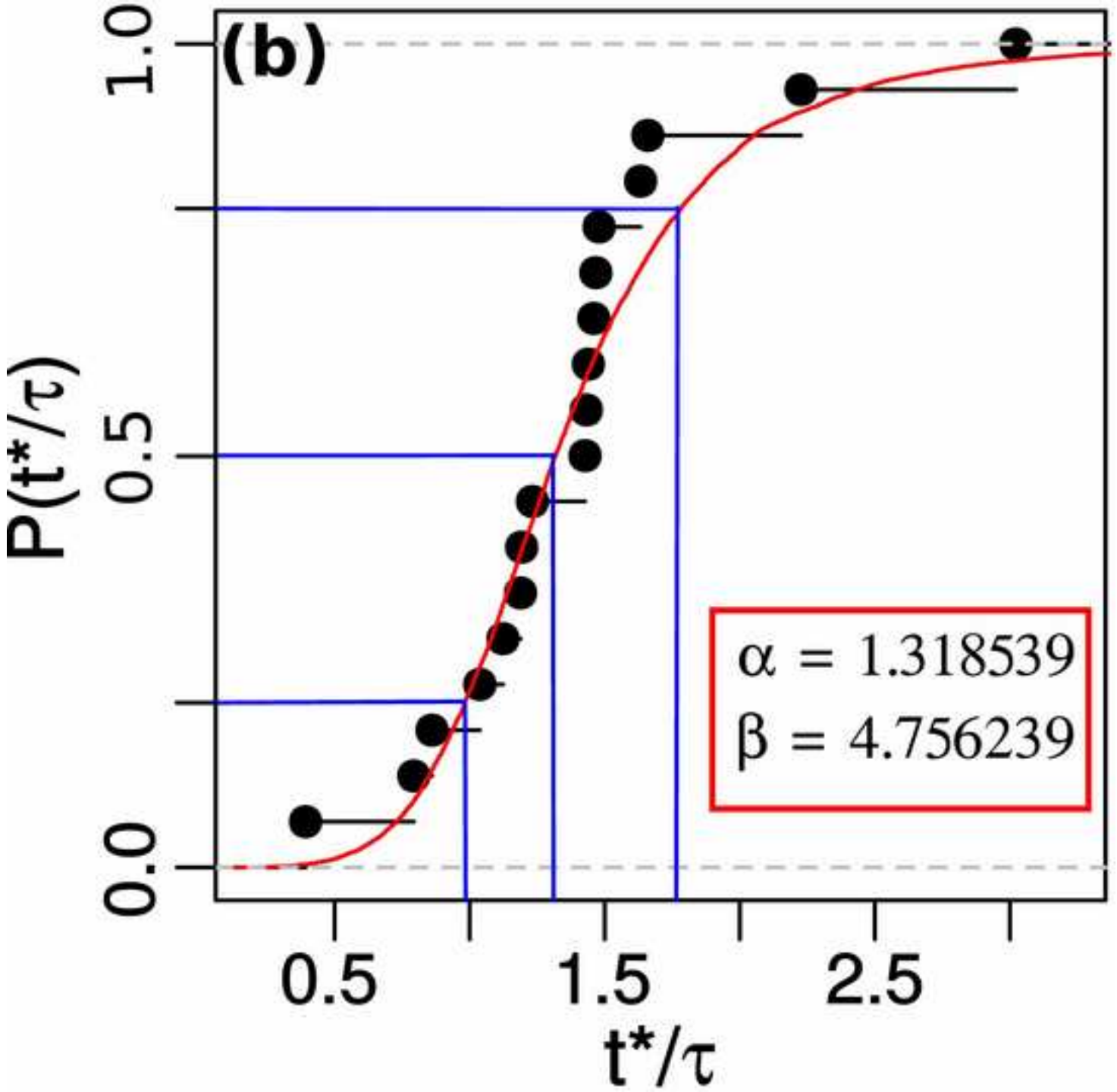

Figure

Click here to download high resolution image

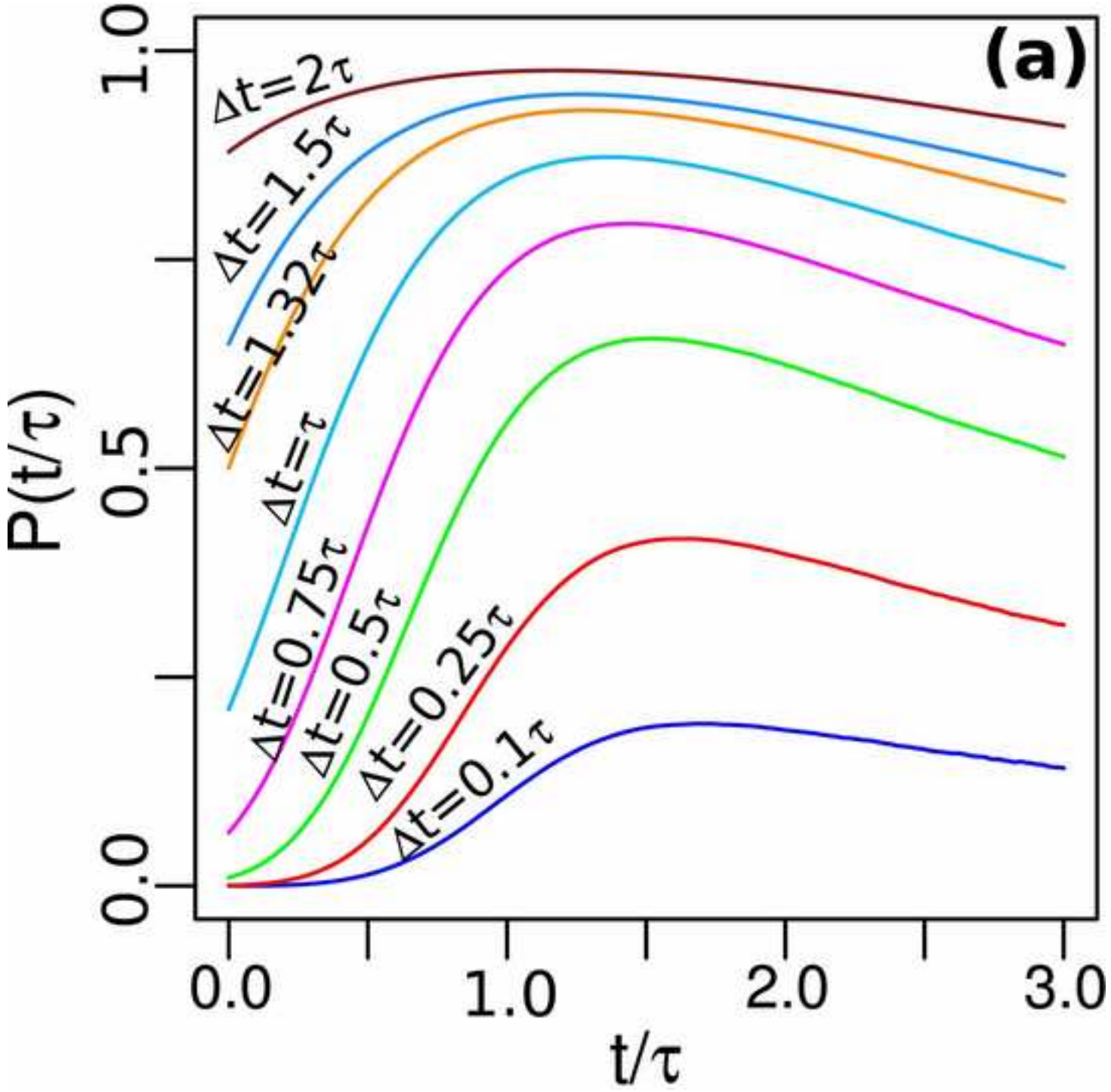

Figure

Click here to download high resolution image

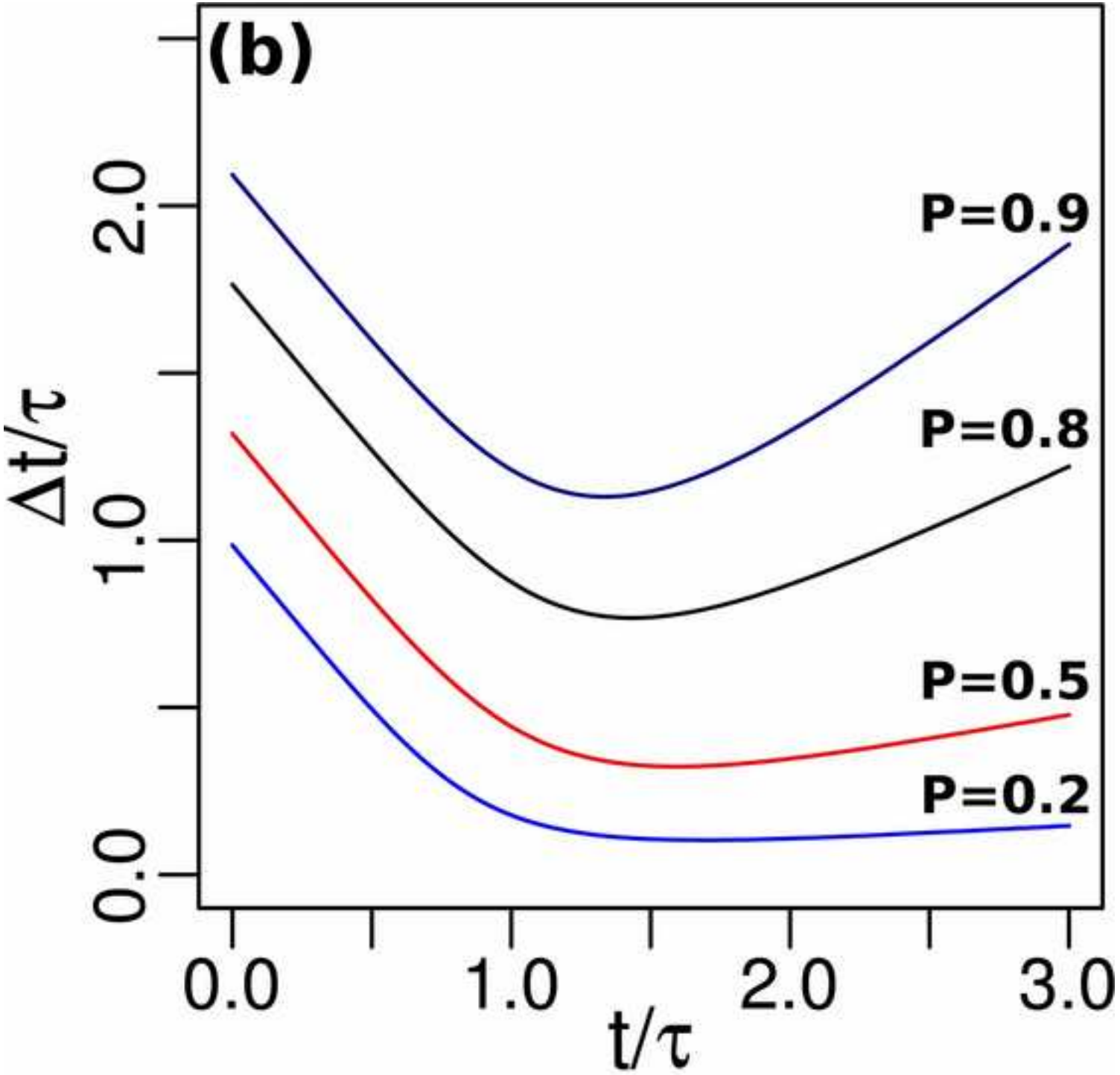

Figure
Click here to download high resolution image

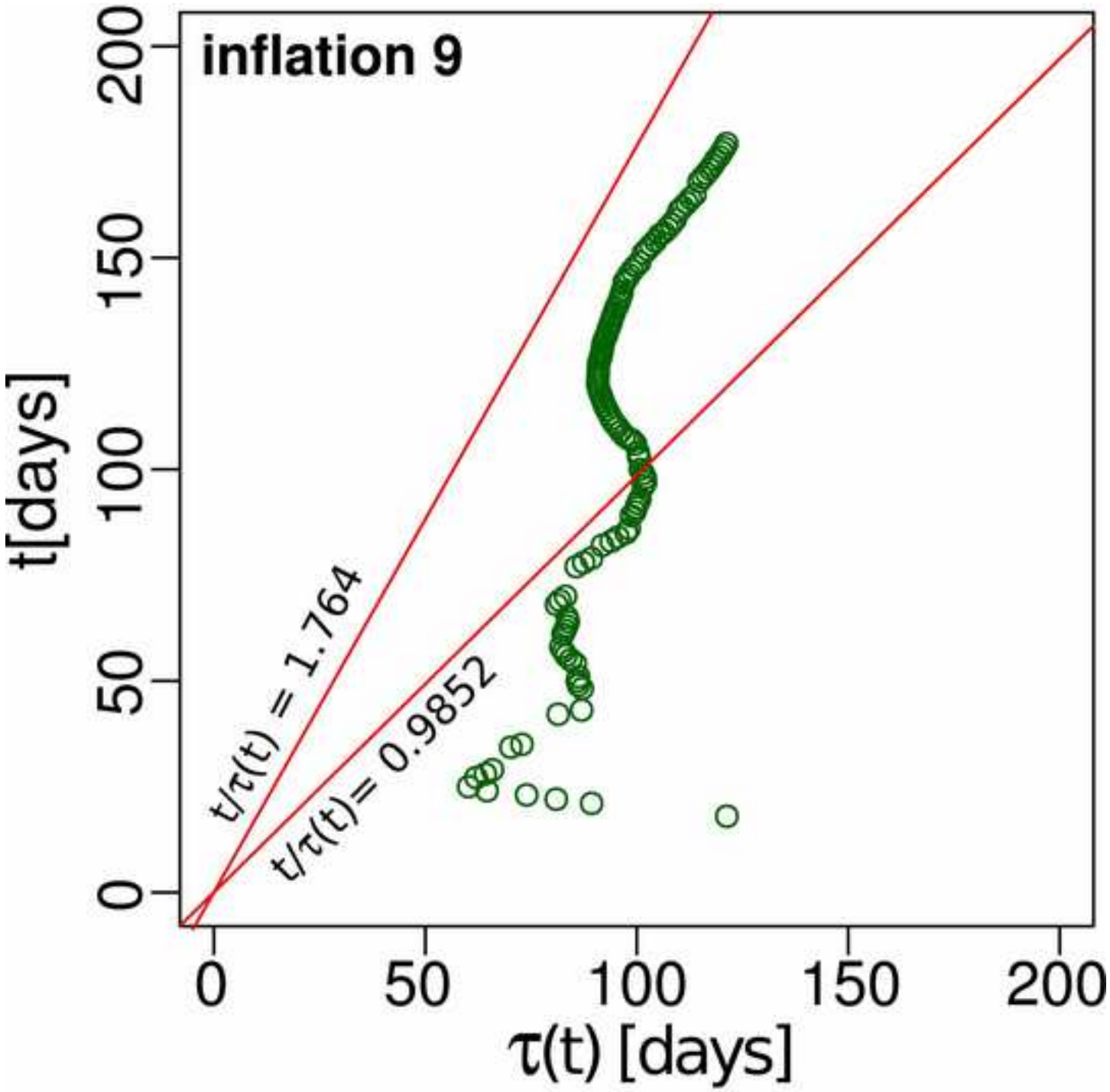

Figure 6

Figure

Click here to download high resolution image

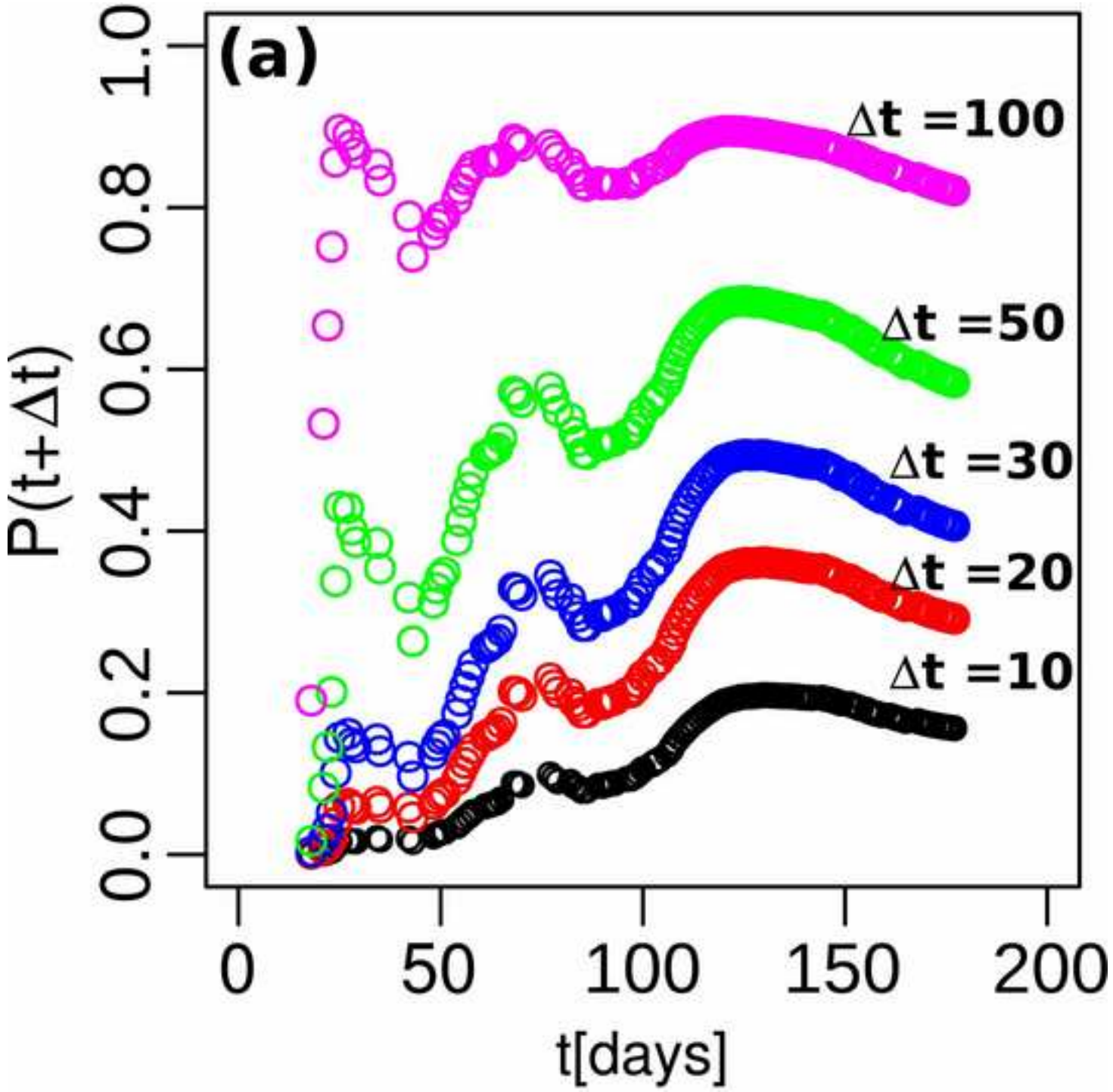

Figure
Click here to download high resolution image

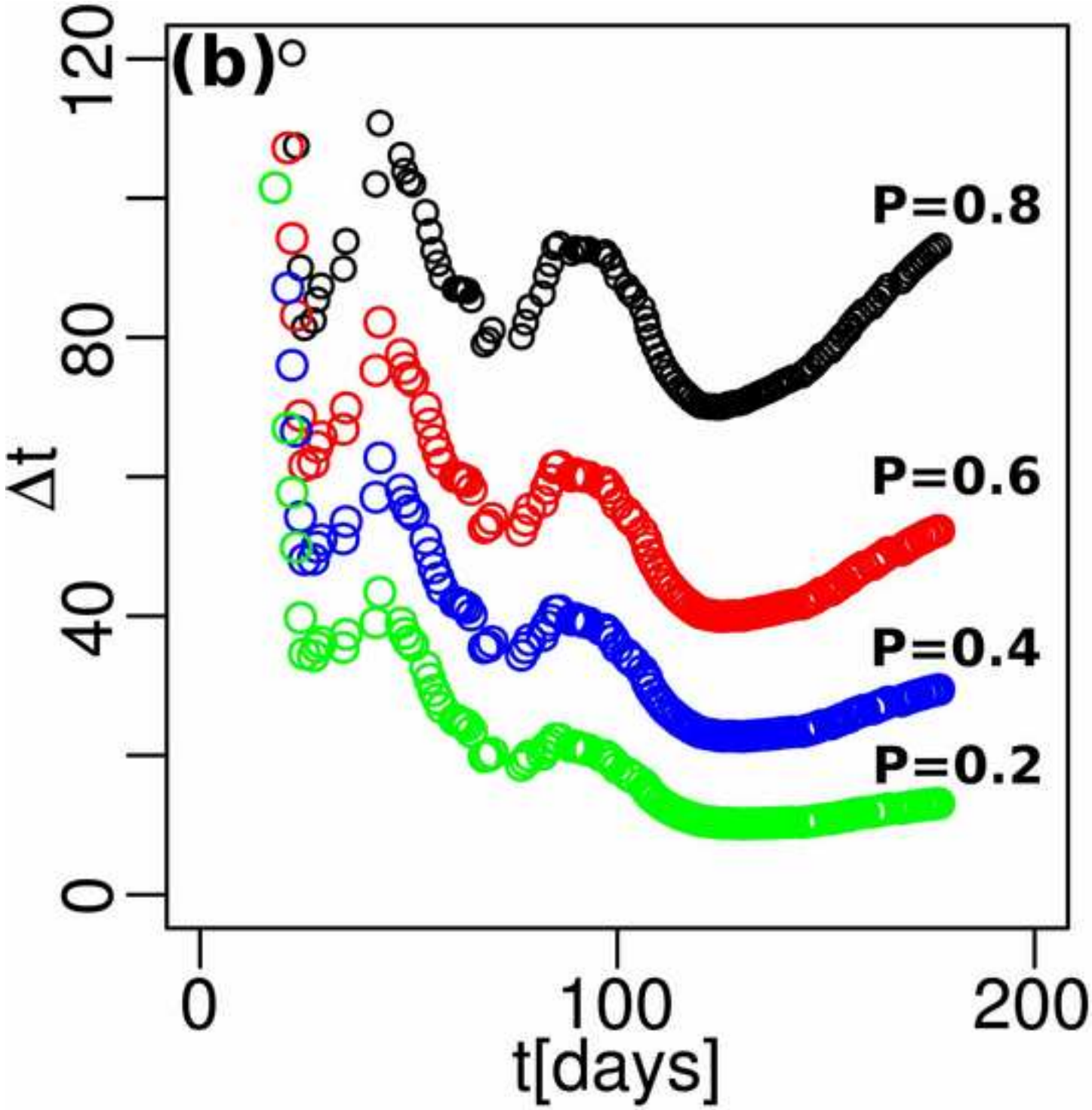

Figure

Click here to download high resolution image

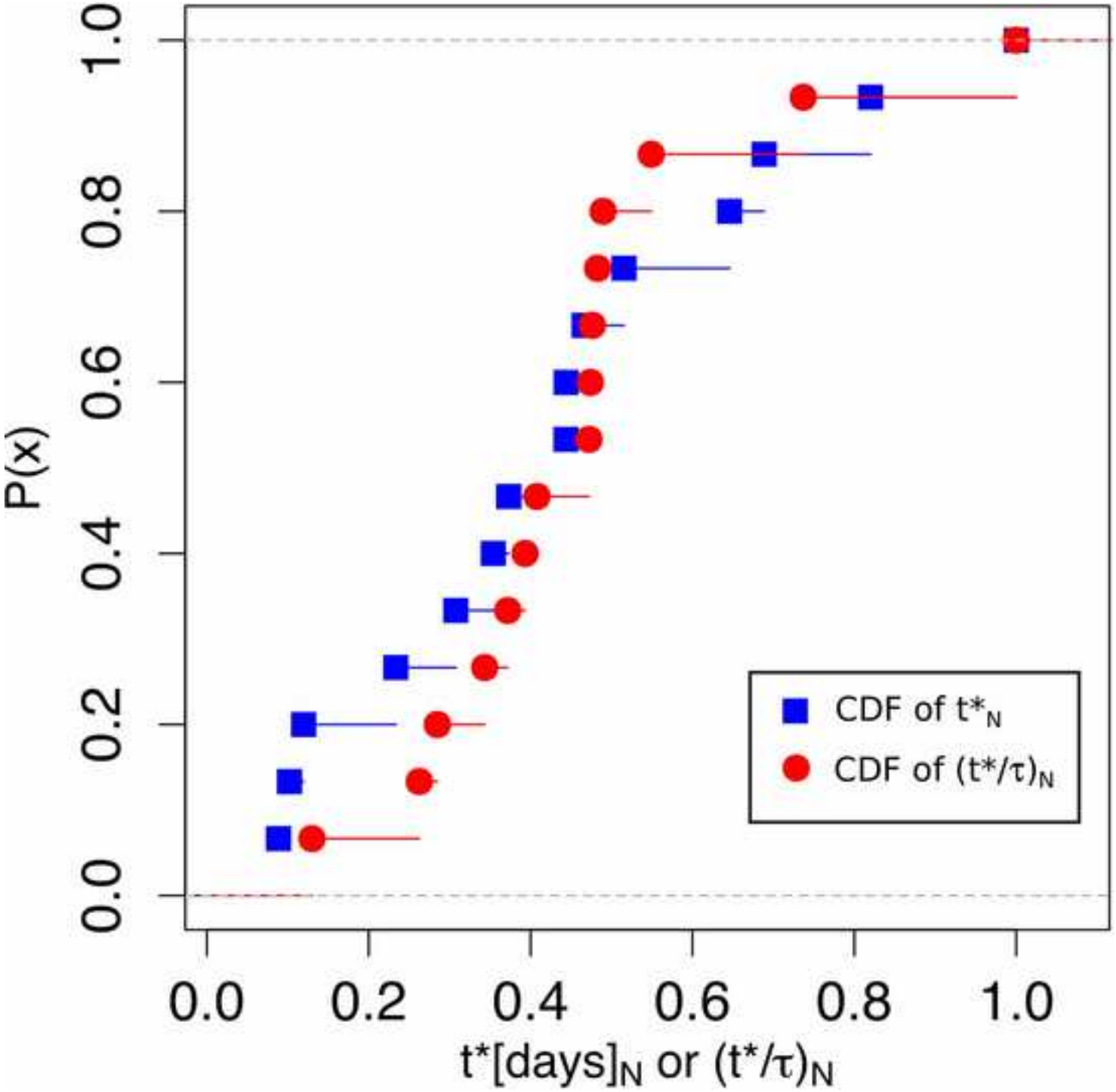

Figure
Click here to download high resolution image

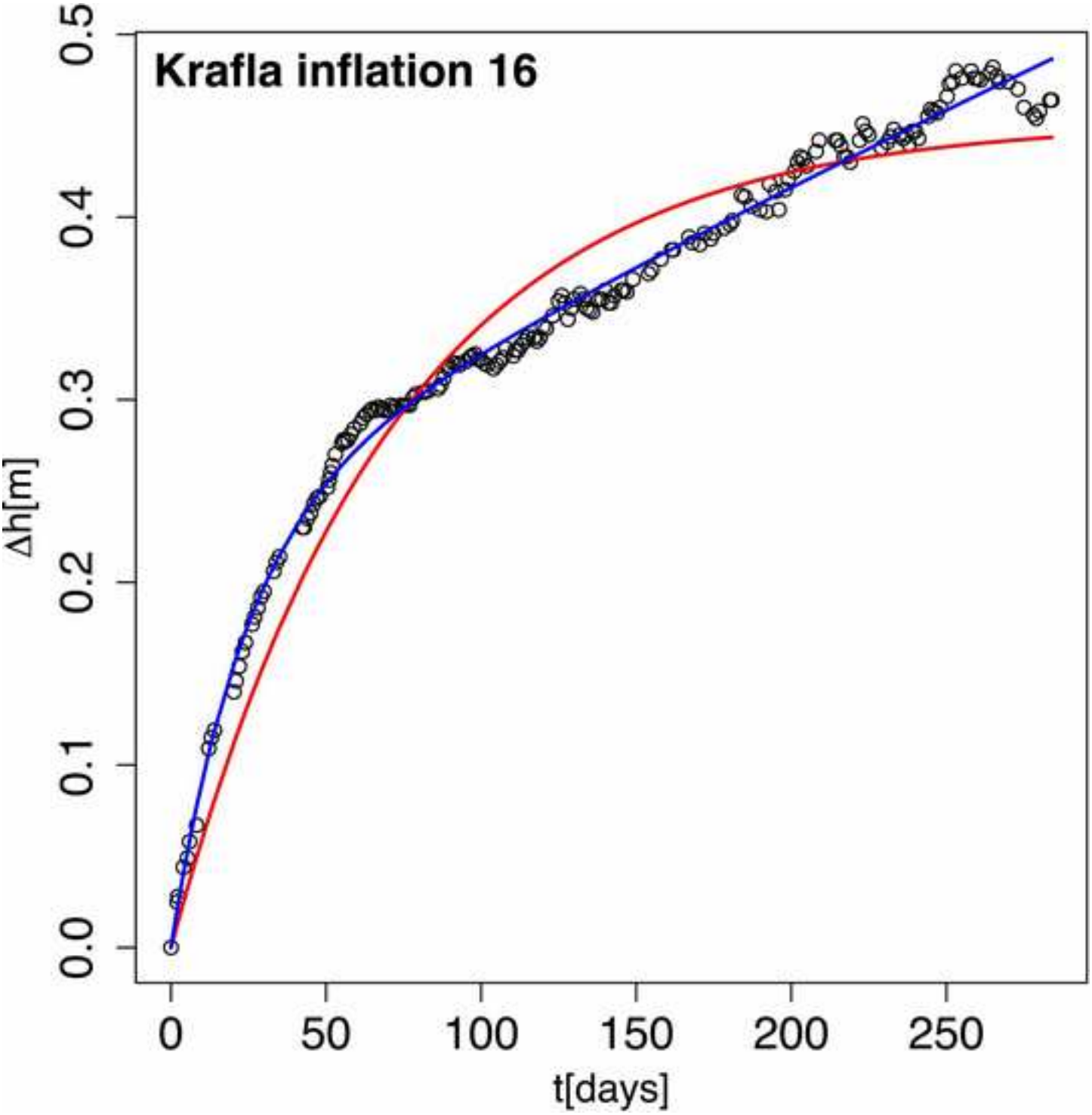

Figure

Click here to download high resolution image